Cell Reports
Physical Science

CellPress

Article

Pressure-induced insulator-to-metal transition in the quantum spin liquid candidate lithium ytterbium diselenide

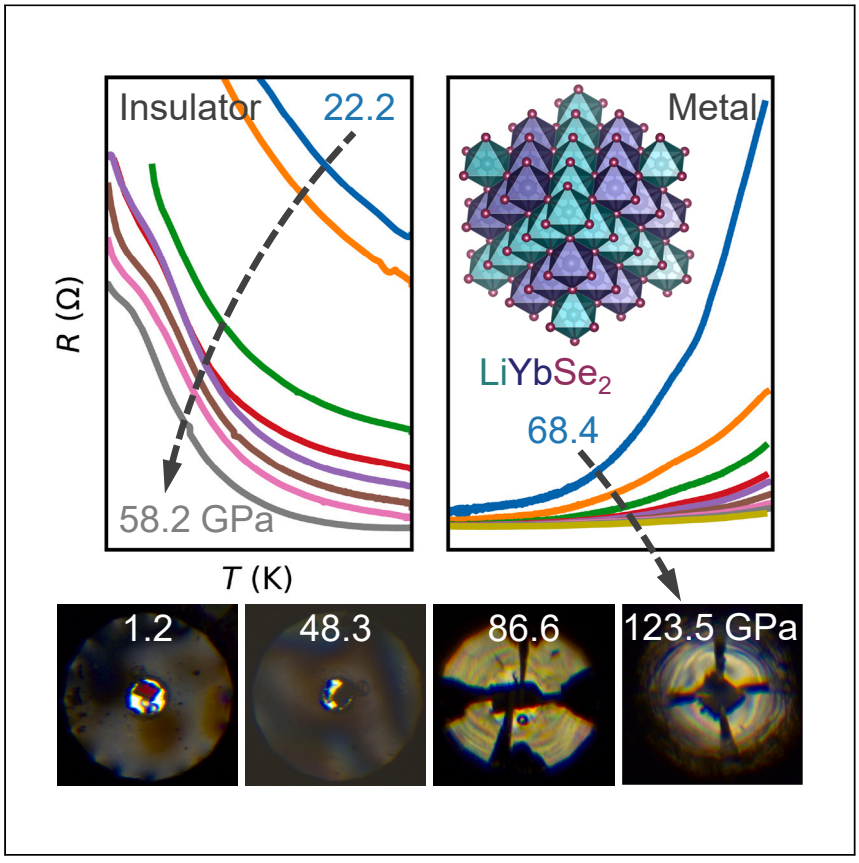

Wang et al. demonstrate how high pressure induces a remarkable transition in $LiYbSe_2$, a quantum spin liquid candidate, from an insulator to a metal. This study sheds light on potential routes to probe the exotic properties of these materials.

Haozhe Wang, Lifen Shi, Shuyuan Huyan, ..., Paul C. Canfield, Jinguang Cheng, Weiwei Xie

jgcheng@iphy.ac.cn (J.C.)
xieweiwe@msu.edu (W.X.)

Highlights

Metallization of quantum spin liquid candidate achieved under high pressure

Absence of structural changes in the studied pressure range

Potential magnetic transitions suggested at higher pressure

Wang et al., Cell Reports Physical Science 5, 101989
June 19, 2024
https://doi.org/10.1016/j.xcrp.2024.101989

Please cite this article in press as: Wang et al., Pressure-induced insulator-to-metal transition in the quantum spin liquid candidate lithium ytterbium diselenide, Cell Reports Physical Science (2024), https://doi.org/10.1016/j.xcrp.2024.101989

Cell Reports
Physical Science

CellPress

Article

Pressure-induced insulator-to-metal transition in the quantum spin liquid candidate lithium ytterbium diselenide

Haozhe Wang,[1,9] Lifen Shi,[2,3,9] Shuyuan Huyan,[4,5] Greeshma C. Jose,[6] Barbara Lavina,[7,8] Sergey L. Bud'ko,[4,5] Wenli Bi,[6] Paul C. Canfield,[4,5] Jinguang Cheng,[2,3,*] and Weiwei Xie[1,10,*]

SUMMARY

Metallization of quantum spin liquid (QSL) materials has long been considered as a potential route toward unconventional superconductivity. Here, we investigate the pressurization of lithium ytterbium diselenide ($LiYbSe_2$), a three-dimensional QSL candidate with a pyrochlore structure. High-pressure X-ray diffraction (up to 15 GPa) and Raman spectroscopy (up to 48 GPa) reveal no significant structural changes within this pressure range. Remarkably insulating, $LiYbSe_2$ exhibits a resistance below 10^5 Ω only at pressures exceeding 25 GPa, accompanied by a gradual reduction of band gap upon compression. Interestingly, an insulator-to-metal transition occurs around 68 GPa, and the metallic behavior persists up to 123.5 GPa, the highest pressure achieved in this study. A possible sign of magnetic transitions is also observed. The insulator-to-metal transition in $LiYbSe_2$ under high pressure presents an ideal platform to explore the pressure effects on QSL candidates of spin-1/2 Yb^{3+} systems with various lattice patterns.

INTRODUCTION

The quantum spin liquid (QSL) state, a highly entangled superposition state of all the possible configurations of valence-bond spin singlets and the spin excitation continuum, has been proposed to understand unconventional superconductivity in high-T_C (high transition temperature) superconductors.[1–4] Geometrically frustrated spin-1/2 (S = 1/2) systems, such as two-dimensional Kagome, triangular, and three-dimensional pyrochlore lattices, are ideal structural platforms to host QSL states.[5–8] Rare earth-based frustrated magnetic systems, for example, $YbMgGaO_4$ with an S = 1/2 Yb^{3+} triangular lattice, have been proposed and studied recently as promising QSL candidates.[9–11] However, the intrinsic structural disorder with a random distribution of Mg^{2+} and Ga^{3+} on one atomic site in $YbMgGaO_4$ may generate a spin-liquid-like state at low temperatures.[12] Thus, $NaYbCh_2$ (Ch = O, S, and Se), which contains a perfect Yb^{3+} triangular lattice, has been proposed and widely explored as an S = 1/2 rare earth-based system without inherent atomic disorders in crystals.[13–15] Our recent work reported that $LiYbSe_2$, an isoelectronic analog of $NaYbSe_2$, suggests a QSL state in which Yb^{3+} adopts an effective S = 1/2 pyrochlore lattice.[16]

High-pressure techniques have been used as a clean tool to induce unconventional superconductivity in QSL candidates.[17,18] For example, an approximate triangular lattice of S = 1/2 Cu^{2+} ions in the organic compound κ-$(BEDT\text{-}TTF)_2Cu_2(CN)_3$ has been proposed theoretically and experimentally examined to host a QSL state.[19] The electron spin resonance measurements down to 50 mK indicated an absence

[1]Department of Chemistry, Michigan State University, East Lansing, MI 48824, USA

[2]Beijing National Laboratory for Condensed Matter Physics and Institute of Physics, Chinese Academy of Sciences, Beijing 100190, China

[3]School of Physical Sciences, University of Chinese Academy of Sciences, Beijing 100190, China

[4]Ames National Laboratory, Iowa State University, Ames, IA 50011, USA

[5]Department of Physics and Astronomy, Iowa State University, Ames, IA 50011, USA

[6]Department of Physics, University of Alabama, Birmingham, AL 35294, USA

[7]Center for Advanced Radiation Sources, The University of Chicago, Chicago, IL 60637, USA

[8]Advanced Photon Source, Argonne National Laboratory, Argonne, IL 60439, USA

[9]These authors contributed equally

[10]Lead contact

*Correspondence: jgcheng@iphy.ac.cn (J.C.), xieweiwe@msu.edu (W.X.)

https://doi.org/10.1016/j.xcrp.2024.101989

Please cite this article in press as: Wang et al., Pressure-induced insulator-to-metal transition in the quantum spin liquid candidate lithium ytterbium diselenide, Cell Reports Physical Science (2024), https://doi.org/10.1016/j.xcrp.2024.101989

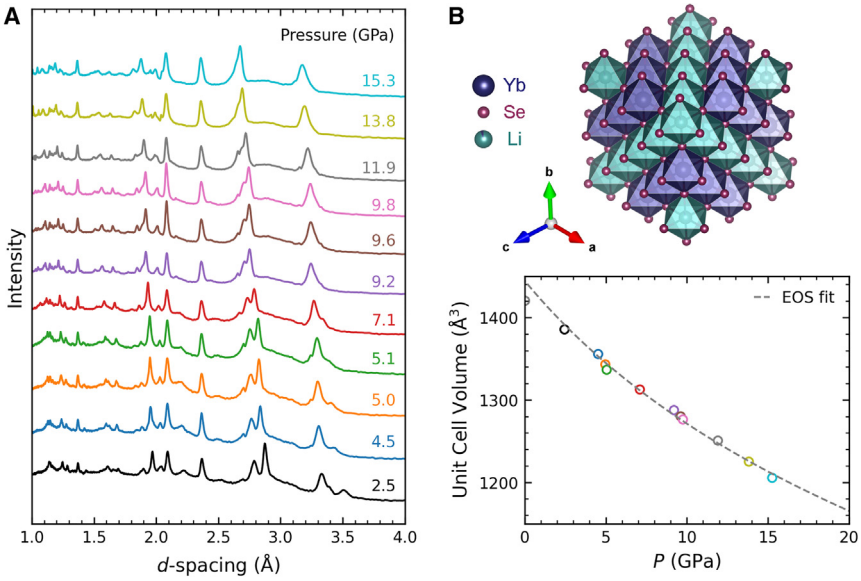

Figure 1. High-pressure powder XRD of $LiYbSe_2$ at room temperature up to 15.3 GPa

(A) Stacked powder XRD pattern at various pressures.

(B) Pressure evolution of unit cell volume and second-order Birch-Murnaghan EOS fit. The crystal structure is also shown.

of magnetic ordering.[20] By applying a very small pressure (~0.35 GPa), the insulator-to-metal transition was observed at around 13 K and followed by a superconducting transition at around 4 K.[21,22] Recently, a high-pressure study was reported on another QSL candidate, $NaYbSe_2$.[23,24] A structural study using X-ray diffraction (XRD) and Raman scattering up to 30 GPa indicates a subtle and collapse-like structural change or valent change on Yb^{3+} without symmetry change at around 12 GPa. The electrical resistance is gradually reduced by applying pressure with a superconducting phase transition occurring at ~5.8 K and ~20 GPa. The metallization trend is confirmed by further high-pressure measurements. These studies inspired us to investigate the resistance changes and possible superconductivity under high pressure in other QSL candidates.[23]

Here, we present the high-pressure studies, including synchrotron XRD, Raman spectroscopy, electrical resistance measurements, and electronic band structure calculations, on $LiYbSe_2$. There are no structural changes in $LiYbSe_2$ observed up to 48 GPa. Interestingly, the electrical resistance measurements confirm that the insulator-to-metal transition occurs around 68 GPa, and a possible sign of a magnetic transition is observed above 90 GPa.

RESULTS AND DISCUSSION

Robust crystal structure at high pressure

Single crystals of $LiYbSe_2$ were grown using the salt flux method (refer to the Supplemental experimental procedures for detailed information). The crystal structure evolution of $LiYbSe_2$ under hydrostatic pressure was studied by performing XRD experiments at room temperature up to 15.3 GPa. As shown in Figure 1A, the cubic pyrochlore structure with the space group *Fd*-3*m* is maintained under pressure. The volume of the unit cell obtained from Rietveld refinements is plotted as the function of pressure in Figure 1B, which shows a smooth contraction upon compression with the lattice parameter *a* changing from 11.242(1) Å at ambient pressure to 10.656(1) Å at 15.3 GPa, further confirming the absence of any structural transition

Please cite this article in press as: Wang et al., Pressure-induced insulator-to-metal transition in the quantum spin liquid candidate lithium ytterbium diselenide, Cell Reports Physical Science (2024), https://doi.org/10.1016/j.xcrp.2024.101989

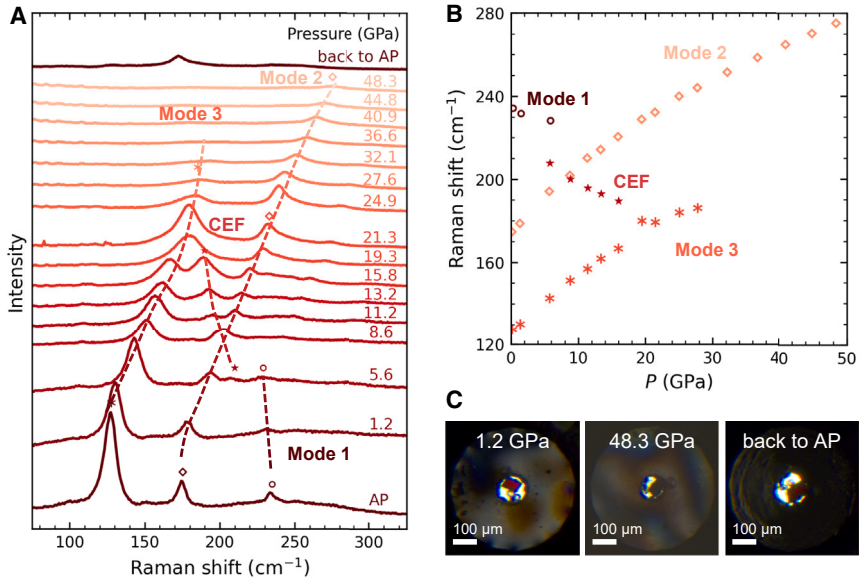

Figure 2. High-pressure Raman spectra of $LiYbSe_2$ up to 48.3 GPa

(A) Stacked Raman spectra at various pressures.

(B) Pressure evolution of Raman vibration modes.

(C) Optical image of the sample under pressure. Scale bar, 100 μm. The color of the crystal becomes darker under pressurization and partially goes back under depressurization.

in the studied pressure range. A least-square fitting to the volume vs. pressure data using the second-order Birch-Murnaghan equation of state (Equation 1) yields the isothermal bulk modulus K_{T_0} = 61(2) GPa and the volume at zero pressure V_0 = 1445(5) Å^3.[25] It should be noted that the standard deviation of the volumes is ~0.4 Å^3 and not visible in Figure 1B.

$$P(V) = \frac{3}{2}K_{T_0}\left[\left(\frac{V_0}{V}\right)^{\frac{7}{3}} - \left(\frac{V_0}{V}\right)^{\frac{5}{3}}\right] \quad \text{(Equation 1)}$$

Crystal electric field excitation observed from Raman spectroscopy

To investigate the bond vibration under high pressure, the Raman spectra under high pressure were taken and summarized in Figure 2A. There are three Raman active modes observed at ~235 cm^{-1} (mode 1), ~175 cm^{-1} (mode 2), and ~128 (mode 3) cm^{-1} at ambient pressure, which is consistent with the Raman active modes of a cubic *Fd*-3*m* structure (origin choice 2) with the 16*c*, 16*d*, and 32*e* sites occupied (A_{1g}, E_g, and T_{2g}). Modes 2 and 3 exhibit a smooth blueshift as the pressure increases. The pressure evolution of Raman modes is summarized in Figure 2B. At ~5.6 GPa, a small peak at 207 cm^{-1} appears. It exhibits a redshift upon pressurization, merging with mode 2 at ~200 cm^{-1} and 8.6 GPa. According to our high-pressure XRD results, no structural transition is observed up to 15.3 GPa; thus, the newly appearing mode is not from the structural distortion and more likely attributable to crystal electric field (CEF) excitation. At about 11.2 GPa, it becomes significantly observable, which may also be considered as the continuous excitation peak from mode 1 crossing mode 2. The intensity of this peak is enhanced at a higher pressure and exhibits a continuous redshift until merged with the peaks of mode 3 at around 180 cm^{-1} and 19.3 GPa. On the other hand, the very weak peak at the higher pressure range (~260 cm^{-1} at 15.8 GPa) can be considered as the extension of mode 1, shown in Figure S1. As another possibility, it might also be caused by spin-phonon coupling, as reported in many rare earth oxides with pyrochlore

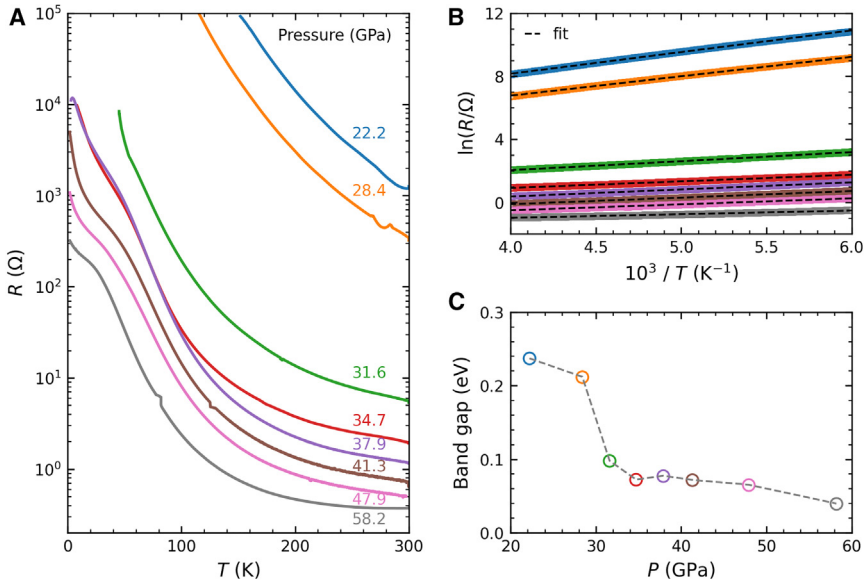

Figure 3. High-pressure electrical resistance of $LiYbSe_2$ up to 58.2 GPa

(A) Temperature dependence of electrical resistance under various pressures. The semiconducting behavior was observed between 22.2 GPa and 58.2 GPa.

(B) The logarithm of electrical resistance plotted as a function of $10^3/T$.

(C) Pressure evolution of the band gap derived from the activation model.

structures.[26] The broad and strong peak of mode 2 is considerably larger in magnitude when compared to the exchange coupling. The broadening of this mode is attributed to resonance and overlaps with phonon frequencies, particularly under high-pressure conditions.[26] As the pressure increases, the peaks in Raman spectra become broader and weaker in intensity as the crystallinity decreases, without the emergence of any other additional peaks up to 48.3 GPa. As shown in Figure 2C, the crystal looks transparent red and turns darker and darker with pressure applied. Once the system was back to ambient pressure, there was only one remaining Raman peak, further confirming the decreased crystallinity. This could also explain the irreversible color change.

Insulator-to-metal transition

To study the electrical transport properties and explore potential superconductivity in $LiYbSe_2$, high-pressure electrical resistance measurements up to 58.2 GPa were performed. The results are shown in Figures 3A and S2. At lower pressure range (<22 GPa), the resistance is too large to be measured in the PPMS. Starting from 22.2 GPa, the resistance can be detected. From 22.2 to 58.2 GPa, $LiYbSe_2$ shows semiconductor-like behavior in the whole temperature range. The resistivity can be described with the Arrhenius activation model, expressed as Equation 2, in which A is a parameter related to the system, Δ_g is the semiconductor band gap, T is temperature, and k_B is Boltzmann constant:

$$\rho = Ae^{\frac{\Delta_g}{2k_BT}} \qquad \text{(Equation 2)}$$

To evaluate the band-gap changes under pressure, the resistance in the temperature range of 165–250 K was fitted accordingly. As shown in Figures 3B and S3, the resistance of the system is roughly described by the activation model, presented as the near-linear correlation between the logarithm of resistance and $10^3/T$ within the range of temperatures under examination. The band gap Δ_g, under different pressures, inferred from these data, is presented in Figure 3C. In general, the

Please cite this article in press as: Wang et al., Pressure-induced insulator-to-metal transition in the quantum spin liquid candidate lithium ytterbium diselenide, Cell Reports Physical Science (2024), https://doi.org/10.1016/j.xcrp.2024.101989

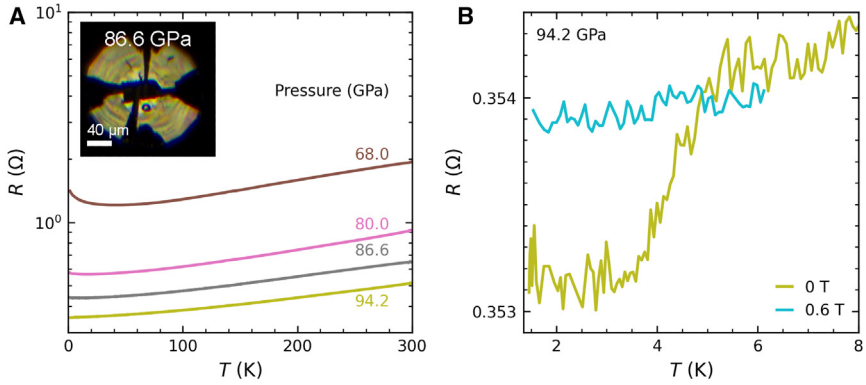

Figure 4. High-pressure electrical resistance of $LiYbSe_2$ up to 94.2 GPa

(A) Temperature dependence of electrical resistance under various pressures. The system becomes metallic around 68.0 GPa. Inset: optical image of the sample at 86.6 GPa. Scale bar, 40 μm.

(B) Electrical resistance at 94.2 GPa with a 0.6-T magnetic field applied.

band gap monotonically decreases with pressure; however, a sudden drop was observed at around 30 GPa, where it decreased from 0.26 eV to below 0.10 eV. This could also be indicated by a dramatic slope change in Figure 3C between 28.4 GPa and 31.6 GPa. Together with the disappearance of Raman active mode 3 in Figure 2, it may indicate that there is a subtle phase transition, such as magnetic transition, in the system at this pressure. As the pressure increases further, the band gap decreases slightly to ~0.02 eV at 58.2 GPa.

To investigate the electrical resistance changes under higher pressure, further measurements were conducted, as shown in Figure 4A. At 68.0 GPa, a metallic behavior was observed with a minimum of around 25 K, which may be caused by a weak localization effect originating from the presence of disorder potentials and incoherent Kondo effect due to the presence of the Yb^{3+} mixture on Li^{+} site.[16,23] As the pressure increases to 80 GPa, the minimum disappears, and a complete metallic behavior in the whole temperature range (1.8–300 K) is achieved. When the experiments were repeated without the pressure-transmitting medium (PTM), the minimum in resistivity was found to be absent. Instead, only a transition from an insulator to a metallic state was observed, as depicted in Figure S4. Such progressive changes at low temperatures and high pressures were also observed in other Yb-series heavy-fermion compounds.[27] $LiYbSe_2$ shows metallic behavior up to 94.2 GPa. The metallization under pressure is also confirmed by the crystal color changes under pressure (Figure 4A, inset). Similar to Figure 2C, the crystal color starts transparent red and becomes darker and darker with pressure, indicating the gradual increase of metallicity. Surprisingly, at 94.2 GPa, a very weak but sudden resistance drop was observed around 5.0 K; in addition, this drop can be eliminated by the application of a 0.6-T magnetic field (Figure 4B). Given the very small size of this drop, the most likely explanation is magnetic transition, but it is also possible that a tiny amount of the second phase (possibly Se) becomes superconducting. Of course, a more enticing option would be the onset of a bulk transition that needed high temperatures to complete. These results motivated us to conduct higher-pressure measurements to explore the potential superconducting or magnetic transition that exists in $LiYbSe_2$.

Potential phase transition observed above 96.0 GPa

The resistance was measured again in another run without PTM, with pressure applied from 68.4 GPa to 123.5 GPa. The results are presented in Figure 5A. As the pressure increased, a very weak drop in resistance was observed, starting at

Please cite this article in press as: Wang et al., Pressure-induced insulator-to-metal transition in the quantum spin liquid candidate lithium ytterbium diselenide, Cell Reports Physical Science (2024), https://doi.org/10.1016/j.xcrp.2024.101989

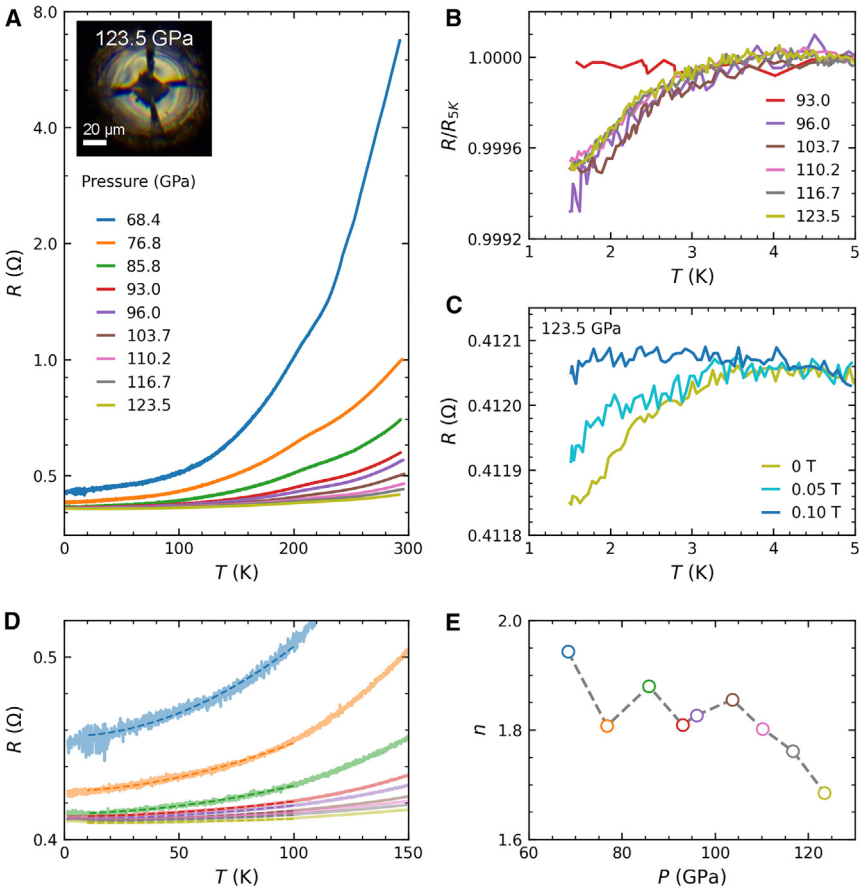

Figure 5. High-pressure electrical resistance of $LiYbSe_2$ up to 123.5 GPa

(A) Temperature dependence of electrical resistance under various pressures. Inset: optical image of the sample at 123.5 GPa. Scale bar, 20 μm.

(B) Normalized electrical resistance at low temperatures under various pressures.

(C) Electrical resistance at 123.5 GPa with a magnetic field applied.

(D) Power-law fitting of electrical resistance under various pressures in the range of 10–100 K.

(E) Pressure dependence of fitted *n* in the metallic state using the power-law equation.

around 3.0 K from 96.0 GPa, as shown in Figure 5B. The potential phase transition temperature is slightly suppressed with pressure from 3.0 K at 96.0 GPa to around 2.5 K at 116.7 GPa. Nevertheless, the size of the anomaly is insufficient to draw any definitive conclusion. At 123.5 GPa, the field-dependent resistance shows that the resistance drop is gradually suppressed, as presented in Figure 5C. At 0.1 T, the transition is completely suppressed, indicating that the drop on the resistance curve at around 3.0 K may originate from the magnetic (antiferromagnetic or some short-range magnetic order) transition. These results strongly suggest that the feature we see is, at best, a very small second phase that might have a superconducting transition and does not represent a bulk phase. It has been observed that the data exhibit discrepancies in the overlapping pressure range, as shown in Figure S4, which can be attributed to variations in the levels of non-hydrostaticity between the two experiment runs. Despite this observation, it is noteworthy that these deviations do not compromise the validity or integrity of the insulator-to-metal transition in $LiYbSe_2$.

In order to understand the metallic state and potential phase transition under pressure, we fitted the resistance data with the power-law equation (Equation 3), where

R_0 is the residual resistance, and the pre-factor A is a parameter related to electron-electron interactions and electron-phonon coupling. Figure 5D shows that the power-law formula fits the experimental data well in the temperature range between 10 K and 100 K. The pressure dependence of the exponent n is plotted in Figure 5E. At the boundary of the insulator-to-metal transition, the metallic state of $LiYbSe_2$ apparently shows a Fermi liquid (FL) ground-state behavior with $n \sim 2$. With pressure increasing, n decreases gradually and approaches $n = 1.68(4)$ at $P = 123.5$ GPa. Therefore, there might be a crossover from FL to non-FL behavior with the increase in pressure approaching the boundary of possible magnetic transition:

$$R(T) = R_0 + AT^n \quad \text{(Equation 3)}$$

In conclusion, we presented high-pressure studies on crystal structure, electrical resistance, and electronic structure (see details in Note S1 and Figure S5) on $LiYbSe_2$ with a cubic pyrochlore lattice. High-pressure powder XRD and Raman spectroscopy reveal no significant structural changes up to 48.3 GPa, confirming that the peak that appeared around 5.6 GPa in Raman spectra originates from CEF excitation. The insulator-to-metal transition was observed around 68.0 GPa in our electrical resistance measurements. The metallic behavior persists up to 123.5 GPa. A low-temperature field-dependent anomaly was detected in the resistance measurements at and above 94.2 GPa, which is most likely related to a magnetic transition. However, under pressure up to 123.5 GPa, no complete structural or even magnetic transition was observed. $LiYbSe_2$ provides an opportunity to study the structure-property relationship and pressure effects in QSL candidates, particularly spin-1/2 Yb^{3+} systems with various lattice patterns.

EXPERIMENTAL PROCEDURES

Resource availability

Lead contact

Requests for further information and resources should be directed to the lead contact, Weiwei Xie (xieweiwe@msu.edu).

Materials availability

The materials used in this study may be available from Weiwei Xie (xieweiwe@msu.edu) with a completed materials transfer agreement. Availability is subject to the current stock in the laboratory.

Data and code availability

The raw data of high-pressure measurements reported in this work are available at https://doi.org/10.5281/zenodo.10988853.

High-pressure synchrotron XRD

The synchrotron powder XRD experiments were carried out up to 15.3 GPa at the Beamline 3ID of the Advanced Photon Source, Argonne National Laboratory. X-rays with a wavelength of 0.4833 Å were focused to 15-μm size. A powder sample ground from single crystals was loaded in a BX90 DAC (Diamond Anvil Cell) with anvils of 400-μm-diameter culet size.[28] Neon was loaded as PTM, and ruby was used to measure pressure *in situ*.[29] The 2D diffraction images were integrated using DIOPTAS software,[30] and Rietveld refinements on the XRD data were performed in GSAS-II.[31]

High-pressure Raman spectrum

To monitor the crystal phase information and bonding interactions in $LiYbSe_2$, the Raman spectra were collected by using a Raman system (spectroscopy and imaging) with 633-nm laser excitation. 4:1 methanol:ethanol was used as the PTM, and the

pressure in DAC was monitored by the R1 fluorescence line of ruby up to 48.3 GPa[32,33]

High-pressure electrical resistance measurements

Ambient pressure to 58.2 GPa pressure range measured at Ames National Laboratory

Electrical resistivity measurement by Van der Pauw method was performed in a commercial diamond anvil cell that fits the Quantum Design Physical Property Measurement System (PPMS). 300-μm culet-size standard-cut diamonds were used as anvils. An $LiYbSe_2$ single crystal of dimensions close to 45 × 45 μm^2 was directly picked out from the sample batch and polished into thin flakes with a thickness of about 15 μm. The sample was loaded together with a tiny piece of ruby ball into the 250-μm-thick, apertured, stainless-steel gasket, which was pre-indented to ∼35 μm, covered by *c*-BN. The sample chamber was about 120 μm in diameter. Platinum foil was used as the electrodes to connect the sample. Mineral oil was used as PTM to provide a better hydrostatic environment at low pressure range. Pressure was determined by the R1 line of the ruby florescent spectrum. Low-temperature resistance measurements down to 1.8 K were conducted in the Quantum Design PPMS.

68.0 GPa–123.5 GPa pressure range measured at the Institute of Physics, Chinese Academy of Sciences

To measure resistance to higher pressure, diamond anvil cells manufactured by HMD with anvils of smaller culet sizes of 200 μm and 100 μm were used. In the first run from 68.0 to 94.2 GPa, the rhenium gasket was pre-indented to ∼34 μm, and then a 60 μm-diameter hole was drilled in the center using a laser drilling system. The rhenium gasket was covered with a *c*-BN epoxy insulating layer. A piece of $LiYbSe_2$ single crystal with dimensions of about 58 × 29 × 12 μm^3 was placed at the center of the sample chamber filled with a KBr PTM.[34] In the second run from 68.4 to 123.5 GPa, the sample with a size of 29 × 29 × 5 μm^3 was placed directly on the *c*-BN epoxy insulating layer at the center of the pre-indented gasket culet without PTM used at all. The pressure was determined by the Raman spectrum of diamond in the whole pressure range.

SUPPLEMENTAL INFORMATION

Supplemental information can be found online at https://doi.org/10.1016/j.xcrp.2024.101989.

ACKNOWLEDGMENTS

The work at Michigan State University was supported by US DOE-BES under contract DE-SC0023648. H.W. and W.X. are thankful for computing resource support from Prof. Gabriel Kotliar at Rutgers University Parallel Computing (RUPC), Center of Materials Theory, Department of Physics and Astronomy. G.C.J. is supported by the NSFC, MOST, and CAS through projects (grants 12025408, 11921004, 2018YFA0305700, and XDB25000000). Part of the high-pressure experiments used the Synergic Extreme Condition User Facility (SECUF). Work at the Ames National Laboratory (S.H., S.L.B., and P.C.C.) was supported by the US Department of Energy (DOE), Office of Science, Basic Energy Sciences, Materials Sciences and Engineering Division under contract DE-AC02-07CH11358. G.C.J. and W.B. acknowledge support from the National Science Foundation (NSF) CAREER Award DMR-2045760. This research used resources of the Advanced Photon Source at the DOE Office of Science user facility operated for the DOE Office of Science by Argonne National Laboratory under contract DE-AC02-06CH11357. Use of the COMPRES-GSECARS gas loading system was supported by COMPRES under NSF

Cooperative Agreement EAR-1606856 and by GSECARS through NSF grant EAR-1634415 and DOE grant DE-FG02-94ER14466.

AUTHOR CONTRIBUTIONS

J.C. and W.X. conceived and supervised the project. H.W., G.C.J., B.L., and W.B. performed high-pressure synchrotron XRD experiments. L.S. and J.C. conducted Raman experiments. L.S., S.H., S.L.B., P.C.C., and J.C. performed high-pressure electrical resistance measurements. H.W. and W.X. analyzed and visualized the data. H.W. and W.X. wrote the manuscript with input from all authors.

DECLARATION OF INTERESTS

The authors declare no competing interests.

Received: January 9, 2024
Revised: March 29, 2024
Accepted: April 29, 2024
Published: May 20, 2024

REFERENCES

1. Savary, L., and Balents, L. (2017). Quantum spin liquids: a review. Rep. Prog. Phys. *80*, 016502. https://doi.org/10.1088/0034-4885/80/1/016502.

2. Broholm, C., Cava, R.J., Kivelson, S.A., Nocera, D.G., Norman, M.R., and Senthil, T. (2020). Quantum spin liquids. Science *367*, eaay0668. https://doi.org/10.1126/science.aay0668.

3. Zhou, Y., Kanoda, K., and Ng, T.-K. (2017). Quantum spin liquid states. Rev. Mod. Phys. *89*, 025003. https://doi.org/10.1103/RevModPhys.89.025003.

4. Chamorro, J.R., McQueen, T.M., and Tran, T.T. (2021). Chemistry of Quantum Spin Liquids. Chem. Rev. *121*, 2898–2934. https://doi.org/10.1021/acs.chemrev.0c00641.

5. Han, T.-H., Helton, J.S., Chu, S., Nocera, D.G., Rodriguez-Rivera, J.A., Broholm, C., and Lee, Y.S. (2012). Fractionalized excitations in the spin-liquid state of a kagome-lattice antiferromagnet. Nature *492*, 406–410. https://doi.org/10.1038/nature11659.

6. Fåk, B., Kermarrec, E., Messio, L., Bernu, B., Lhuillier, C., Bert, F., Mendels, P., Koteswararao, B., Bouquet, F., Ollivier, J., et al. (2012). Kapellasite: A Kagome Quantum Spin Liquid with Competing Interactions. Phys. Rev. Lett. *109*, 037208. https://doi.org/10.1103/PhysRevLett.109.037208.

7. Norman, M.R. (2016). Colloquium: Herbertsmithite and the search for the quantum spin liquid. Rev. Mod. Phys. *88*, 041002. https://doi.org/10.1103/RevModPhys.88.041002.

8. Itou, T., Oyamada, A., Maegawa, S., Tamura, M., and Kato, R. (2008). Quantum spin liquid in the spin-1/2 triangular antiferromagnet $EtMe_3Sb[Pd(dmit)_2]_2$. Phys. Rev. B *77*, 104413. https://doi.org/10.1103/PhysRevB.77.104413.

9. Paddison, J.A.M., Daum, M., Dun, Z., Ehlers, G., Liu, Y., Stone, M.B., Zhou, H., and Mourigal, M. (2017). Continuous excitations of the triangular-lattice quantum spin liquid $YbMgGaO_4$. Nat. Phys. *13*, 117–122. https://doi.org/10.1038/nphys3971.

10. Shen, Y., Li, Y.-D., Wo, H., Li, Y., Shen, S., Pan, B., Wang, Q., Walker, H.C., Steffens, P., Boehm, M., et al. (2016). Evidence for a spinon Fermi surface in a triangular-lattice quantum-spin-liquid candidate. Nature *540*, 559–562. https://doi.org/10.1038/nature20614.

11. Li, Y., Adroja, D., Biswas, P.K., Baker, P.J., Zhang, Q., Liu, J., Tsirlin, A.A., Gegenwart, P., and Zhang, Q. (2016). Muon Spin Relaxation Evidence for the U(1) Quantum Spin-Liquid Ground State in the Triangular Antiferromagnet $YbMgGaO_4$. Phys. Rev. Lett. *117*, 097201. https://doi.org/10.1103/PhysRevLett.117.097201.

12. Huang, Y.Y., Xu, Y., Wang, L., Zhao, C.C., Tu, C.P., Ni, J.M., Wang, L.S., Pan, B.L., Fu, Y., Hao, Z., et al. (2021). Heat Transport in Herbertsmithite: Can a Quantum Spin Liquid Survive Disorder? Phys. Rev. Lett. *127*, 267202. https://doi.org/10.1103/PhysRevLett.127.267202.

13. Liu, W., Zhang, Z., Ji, J., Liu, Y., Li, J., Wang, X., Lei, H., Chen, G., and Zhang, Q. (2018). Rare-Earth Chalcogenides: A Large Family of Triangular Lattice Spin Liquid Candidates. Chin. Phys. Lett. *35*, 117501. https://doi.org/10.1088/0256-307x/35/11/117501.

14. Dai, P.-L., Zhang, G., Xie, Y., Duan, C., Gao, Y., Zhu, Z., Feng, E., Tao, Z., Huang, C.-L., Cao, H., et al. (2021). Spinon Fermi Surface Spin Liquid in a Triangular Lattice Antiferromagnet $NaYbSe_2$. Phys. Rev. X *11*, 021044. https://doi.org/10.1103/PhysRevX.11.021044.

15. Zhang, Z., Ma, X., Li, J., Wang, G., Adroja, D.T., Perring, T.P., Liu, W., Jin, F., Ji, J., Wang, Y., et al. (2021). Crystalline electric field excitations in the quantum spin liquid candidate $NaYbSe_2$. Phys. Rev. B *103*, 035144. https://doi.org/10.1103/PhysRevB.103.035144.

16. Dissanayaka Mudiyanselage, R.S., Wang, H., Vilella, O., Mourigal, M., Kotliar, G., and Xie, W. (2022). $LiYbSe_2$: Frustrated Magnetism in the Pyrochlore Lattice. J. Am. Chem. Soc. *144*, 11933–11937. https://doi.org/10.1021/jacs.2c02839.

17. Cava, R., de Leon, N., and Xie, W. (2021). Introduction: Quantum Materials. Chem. Rev. *121*, 2777–2779. https://doi.org/10.1021/acs.chemrev.0c01322.

18. Tokura, Y., Kawasaki, M., and Nagaosa, N. (2017). Emergent functions of quantum materials. Nat. Phys. *13*, 1056–1068. https://doi.org/10.1038/nphys4274.

19. Geiser, U., Wang, H.H., Carlson, K.D., Williams, J.M., Charlier, H.A., Jr., Heindl, J.E., Yaconi, G.A., Love, B.J., and Lathrop, M.W. (1991). Superconductivity at 2.8 K and 1.5 kbar in κ-$(BEDT\text{-}TTF)_2Cu_2(CN)_3$: the first organic superconductor containing a polymeric copper cyanide anion. Inorg. Chem. *30*, 2586–2588. https://doi.org/10.1021/ic00012a005.

20. Miksch, B., Pustogow, A., Rahim, M.J., Bardin, A.A., Kanoda, K., Schlueter, J.A., Hübner, R., Scheffler, M., and Dressel, M. (2021). Gapped magnetic ground state in quantum spin liquid candidate κ-$(BEDT\text{-}TTF)_2Cu_2(CN)_3$. Science *372*, 276–279. https://doi.org/10.1126/science.abc6363.

21. Rösslhuber, R., Pustogow, A., Uykur, E., Böhme, A., Löhle, A., Hübner, R., Schlueter, J.A., Tan, Y., Dobrosavljević, V., and Dressel, M. (2021). Phase coexistence at the first-order Mott transition revealed by pressure-dependent dielectric spectroscopy of κ-$(BEDT\text{-}TTF)_2Cu_2(CN)_3$. Phys. Rev. B *103*, 125111. https://doi.org/10.1103/PhysRevB.103.125111.

22. Komatsu, T., Matsukawa, N., Inoue, T., and Saito, G. (1996). Realization of Superconductivity at Ambient Pressure by Band-Filling Control in κ-$(BEDT\text{-}TTF)_2Cu_2(CN)_3$. J. Phys. Soc. Jpn. *65*, 1340–1354. https://doi.org/10.1143/JPSJ.65.1340.

23. Jia, Y.-T., Gong, C.-S., Liu, Y.-X., Zhao, J.-F., Dong, C., Dai, G.-Y., Li, X.-D., Lei, H.-C., Yu,

R.-Z., Zhang, G.-M., and Jin, C.-Q. (2020). Mott Transition and Superconductivity in Quantum Spin Liquid Candidate $NaYbSe_2$. Chin. Phys. Lett. *37*, 097404. https://doi.org/10.1088/0256-307x/37/9/097404.

24. Xu, Y., Sheng, Y., and Yang, Y.-f. (2022). Mechanism of the insulator-to-metal transition and superconductivity in the spin liquid candidate $NaYbSe_2$ under pressure. npj Quantum Mater. *7*, 21. https://doi.org/10.1038/s41535-022-00429-7.

25. Katsura, T., and Tange, Y. (2019). A Simple Derivation of the Birch–Murnaghan Equations of State (EOSs) and Comparison with EOSs Derived from Other Definitions of Finite Strain. Minerals *9*, 745. https://doi.org/10.3390/min9120745.

26. Rao, X., Hussain, G., Huang, Q., Chu, W.J., Li, N., Zhao, X., Dun, Z., Choi, E.S., Asaba, T., Chen, L., et al. (2021). Survival of itinerant excitations and quantum spin state transitions in $YbMgGaO_4$ with chemical disorder. Nat. Commun. *12*, 4949. https://doi.org/10.1038/s41467-021-25247-6.

27. Yuan, H.Q., Nicklas, M., Hossain, Z., Geibel, C., and Steglich, F. (2006). Quantum phase transition in the heavy-fermion compound $YbIr_2Si_2$. Phys. Rev. B *74*, 212403. https://doi.org/10.1103/PhysRevB.74.212403.

28. Kantor, I., Prakapenka, V., Kantor, A., Dera, P., Kurnosov, A., Sinogeikin, S., Dubrovinskaia, N., and Dubrovinsky, L. (2012). BX90: A new diamond anvil cell design for X-ray diffraction and optical measurements. Rev. Sci. Instrum. *83*, 125102. https://doi.org/10.1063/1.4768541.

29. Dewaele, A., Torrent, M., Loubeyre, P., and Mezouar, M. (2008). Compression curves of transition metals in the Mbar range: Experiments and projector augmented-wave calculations. Phys. Rev. B *78*, 104102. https://doi.org/10.1103/PhysRevB.78.104102.

30. Prescher, C., and Prakapenka, V.B. (2015). DIOPTAS: a program for reduction of two-dimensional X-ray diffraction data and data exploration. High Press. Res. *35*, 223–230. https://doi.org/10.1080/08957959.2015.1059835.

31. Toby, B.H., and Von Dreele, R.B. (2013). GSAS-II: the genesis of a modern open-source all purpose crystallography software package. J. Appl. Crystallogr. *46*, 544–549. https://doi.org/10.1107/S0021889813003531.

32. Shen, G., Wang, Y., Dewaele, A., Wu, C., Fratanduono, D.E., Eggert, J., Klotz, S., Dziubek, K.F., Loubeyre, P., Fat'yanov, O.V., et al. (2020). Toward an international practical pressure scale: A proposal for an IPPS ruby gauge (IPPS-Ruby2020). High Press. Res. *40*, 299–314. https://doi.org/10.1080/08957959.2020.1791107.

33. Hu, Q., and Mao, H.-k. (2021). Born's valence force-field model for diamond at terapascals: Validity and implications for the primary pressure scale. Matter Radiat. Extremes *6*, 068403. https://doi.org/10.1063/5.0069479.

34. Celeste, A., Borondics, F., and Capitani, F. (2019). Hydrostaticity of pressure-transmitting media for high pressure infrared spectroscopy. High Press. Res. *39*, 608–618. https://doi.org/10.1080/08957959.2019.1666844.